Numerical investigation into the inclination effect on conjugate pool boiling and the condensation of steam in a passive heat removal system

S. M. A. Noori Rahim Abadi, J. P. Meyer*

Department of Mechanical and Aeronautical Engineering, University of Pretoria,

Pretoria, South Africa

*Corresponding author's email: josua.meyer@up.ac.za

Tel: +27 0 12 420 3104; Fax: +27 0 12 362 5124

Abstract:

In this study, the effect of the tube inclination angle on simultaneous condensation inside and pool boiling outside a smooth tube is investigated numerically. Such conjugate phase-change phenomena happen in many heat exchangers, particularly in passive heat removal systems. The simulated domain is a pool filled with water liquid at atmospheric pressure, with a submerged tube with inner and outer diameters of 19 mm and 25 mm respectively. The fluid inside the tube is considered to be the steam at the saturation temperature of 250 °C, which is a very common operating condition in many heat removal systems. The flow field is considered to be turbulent, unsteady and three dimensional. The effect of conduction through the tube thickness is also taken into account. The Eulerian-Eulerian multiphase flow approach is utilized to express the governing equation of the problem. ANSYS FLUENT 17.1 is also used to solve the governing equations. The effects of various parameters, such as tube orientation, steam mass flux and inlet steam quality on the condensation and pool boiling heat transfer coefficients, are investigated. The results show good agreement with the available experimental data. The condensation heat transfer coefficient is found to increase with an increase in the inlet steam quality and steam mass flow rate. The results of the effect of inclination on the heat transfer coefficient are also compatible with the previous experimental works. Moreover, the results show that there is a partial maximum point for the total heat transfer coefficient at an inclination angle between θ = -60° and θ = -30°.

Keywords: Pool boiling, condensation, Eulerian-Eulerian, RPI model, inclination angle.

Nomenclature:

a_b	Part of the wall surface covered by nucleate bubbles
$A_{interfacial}$	Interfacial area concentration
C_D	Drag coefficient
C_L	Lift coefficient
C_p	Specific heat
d	Bubble diameter
D_w	Bubble departure diameter
Eo	Eotvos number
f	Drag function
F	Force
g	Gravitational acceleration
G	Mass flux
G_b	Generation of turbulence kinetic energy due to buoyancy
h	Fluid specific enthalpy
$h_{condensation}$	Condensation Heat transfer coefficient
$h_{pool\ boiling}$	Boiling heat transfer coefficient
h_{lv}	Latent heat of evaporation
h_c	Single-phase heat transfer coefficient
I	3×3 identity matrix
k	Thermal conductivity
L	Tube length
$\dot{m}$	Mass transfer rate

Mo	Morton number
n	Number of phases
Nu	Nusselt number
N_w	Nucleate site density
P	Pressure
ΔP	Pressure drop
Pr	Prandtl number
$\dot{q}$	Heat flux
$\dot{q}_C$	Convective heat flux
$\dot{q}_Q$	Quenching heat flux
$\dot{q}_E$	Evaporative heat flux
Q	Intensity of heat exchange between the different phases
r	Radius
$\vec{R}$	Interphase momentum force
Re	Reynolds number
$\vec{u}$	Velocity
S	Mass transfer source term
Sc	Schmidt number
S_u	Momentum source term
S_h	Energy source term
t	Time
T	Temperature
U_t	Tangential component of the velocity vector

x_{in}	Inlet steam mass fraction
y	Distance to wall

Greek symbols

τ	Period of the bubble detachment process
$\bar{\bar{\tau}}$	Stress tensor
α	Volume fraction
ρ	Density
μ	Viscosity
λ	Bulk viscosity
κ	Turbulent kinetic energy
ε	Turbulent energy dissipation rate
Ω	Mean rate of rotation tensor
σ	Surface tension
δt	Time scale in boiling model
θ	Tube inclination angle
$\bar{\Omega}_{ij}$	Mean rate of rotation tensor
φ	Rotation angle
ω	Angular velocity

Subscripts

b	Bubble
i	Phase index
j	Phase index
l	Liquid

lv	Liquid-vapour
L	Laminar
m	Mixture
sat	Saturation
t	Turbulent
v	Vapour
v,m	Virtual mass
w	Wall

1. Introduction

A heat removal system that operates without any power supply allows passive heat removal from the containment to a water pool outside the containment. Steam inside the containment atmosphere condenses at the surface of the heat exchanger, and heat is transferred to the outside pool by single- or two-phase natural circulation. With this component, the containment pressure is kept below the design pressure and remains stable at a low pressure, even in the long term, as long as the water reservoir outside the containment is available [1].

Numerous studies have been conducted on condensation inside horizontal [2-6] and inclined [7-10] tubes. Moreover, many researchers have investigated the pool boiling phenomenon outside the tubes and the tube bundle [11-15].

Pool boiling phenomenon, were experimentally investigated by Gorgy and Eckels [16] who determined the local heat transfer coefficients for R-134a pool boiling on smooth and enhanced

tubes. The heat flux needed to induce pool boiling was provided by warm water flowing inside the tubes. For the enhanced tube, two distinctive regions were detected in the pool boiling curve. Across the first region, the heat transfer coefficient rised sharply with heat flux. In the second region, the heat transfer coefficient was independent of the heat flux; as a result, both regions of the pool boiling curve could be accurately modelled using a proper power law model. Nucleate pool boiling from a small staggered tube bundle flooded in water, methanol and refrigerant R141b was evaluated via an experiment by Krasowski and Cieslinski [17]. The highest total heat transfer coefficient was determined for the case of a tube bundle flooded in water and operating under atmospheric conditions. Moreover, these researchers determined that as the pitch-to-diameter ratio of the tube bundle increased, the heat transfer coefficient increased as well.

Meyer and his co-workers [8-10] experimentally studied the effect of the inclination angle on the condensation inside a smooth tube. They investigated this effect on the pressure drop, void fraction, and heat transfer coefficient, and also captured the flow regime at the tube outlet. Their most important result was that the optimum heat transfer coefficients occurred at a downward inclination angle of 15° - 30°, specifically at mass fluxes lower than approximately 200 kg/m^2s. Shah [7] proposed a method for the calculation of heat transfer coefficients inside inclined tubes during condensation. The method had a mean absolute deviation of 15.7% with the available database. The proposed method is widely used many industrial applications.

Besides the studies on condensation and pool boiling, some researchers have worked on the performance of passive heat removal systems numerically [18-20] and experimentally [21, 22], in which both phenomena take place simultaneously.

Most of the previous works in this field were experimental studies. Wu *et al.* [23] experimentally investigated the effects of the main parameters on the passive heat removal systems using a two-phase natural circulation test facility. The experimental results showed that the natural circulation system was feasible in removing the decay heat, even though some fluctuations, such as intermittent boiling, may occur in the operation. They also found that intermittent boiling and density wave oscillation might occur at a low heat flux, but the instabilities did not have a severe impact on the system operation due to their small amplitudes. Wu *et al.* [24] experimentally studied the overall performance sensitivity of the passive heat removal system in a high-pressure water reactor. Their case study showed that natural circulation can be maintained at different pressures, from one pressure point to another, in the power drop condition as well. The results showed that the system can be used to remove the decay heat as expected. Chen *et al.* [25] experimentally studied the performance of the drain tank cooling in the passive heat removal system in a molten salt reactor. They found that the boiling heat transfer coefficient was not the main factor to improve the overall heat transfer capacity. Moreover, their results showed that, due to the large temperature difference, radiation heat transfer plays a significant role between the thimble and the bayonet tube. Nie *et al.* [26] conducted an experimental investigation on high-pressure steam condensation inside a tube with pool boiling outside. Their results showed that the outer wall temperature distribution was not uniform in the circumferential direction, and the wall temperature and heat flux increased with pressure, mass velocity and steam quality. They also found that the condensation heat transfer coefficient and frictional pressure drop increased as the steam mass flux and quality increased, but decreased with saturation pressure. Moreover, they proposed a modified

correlation from Akers *et al.* [27] for predicting the condensation heat transfer coefficient of high-pressure steam inside a tube.

Conducting experiments for passive heat removal system would be very expensive and time-consuming, therefore numerical methods as an alternative attracted a lot of interests during the past years. Although there are also some numerical works on the performance assessment of passive heat removal systems, none of them considered condensation and pool boiling simultaneously. Minocha *et al.* [28] numerically studied the performance of a passive heat removal system at different tube inclination angles using Open Foam solver. They found that the heat transfer coefficient increased with an increase in the tube inclination angle. The heat transfer was found to be at its maximum for $\theta = 90°$ and at its minimum for $\theta = 15°$. They deduced that this behaviour was due to the interaction between the primary flow (due to the pressure gradient) and the secondary flow (due to the buoyancy force). The primary flow enhanced the fluid's sliding motion at the top of the tube, whereas the secondary flow resulted in an enhancement of the fluid motion along the circumference of tube. Minocha *et al.* [29] extended their work and performed a three-dimensional (3D) numerical simulation for the prediction of a heat removal system at various tube inclination angles (θ) using a mixture two-phase flow formulation. They only considered pool boiling outside the tube and imposed a constant heat flux at the tube wall. They found that the major heat transfer mechanism was liquid agitation caused by sliding bubbles on the tube's surface. In contrast to their single-phase simulations, their results showed that the heat transfer was at its maximum at $\theta = 75°$ and at its minimum at $\theta = 30°$. Dijo *et al.* [30] studied the sodium-cooled fast reactor pool using single-phase two-dimensional (2D) axisymmetric numerical simulation. The study showed that the pool of cold sodium played a significant role in decay heat removal. The

results also revealed that the heat removed by the side pool proved to be more significant in terms of its magnitude.

Furthermore, research has been conducted on the performance assessment of passive heat removal systems by conducting thermal-hydraulic calculations [31, 32]. Ayhan and Sökmen [33] performed thermal-hydraulic calculations of a passive residual heat removal system (PRHRS) with a finned heat exchanger. They considered the effects of various fin parameters, such as thickness, fin radius and total number of fins, in their calculations. Their results showed that the most important fin parameter was the fin radius. As the fin radius increased, the required tube length decreased. They also found that the optimum fin pitch was 3. The study also showed that 2% of nominal reactor power could be removed by the proposed design. Wu *et al.* [19] proposed a numerical model to investigate the use of the passive system and investigate the interaction between the boiling loop and the condensing loop at steady-state conditions. The results showed that the mass flow rate in the boiling loop does indeed have a maximum value. Both the maximum value and the system pressure are mainly affected by the heat flux and heat transfer capacity of the condenser. The mass flow rate in the condensing loop is controlled by heat flux instead of other parameters, thus it seems that the condensing loop is a follower of the boiling loop. Damiani *et al.* [34] proposed a passive heat removal system with the use of MATLAB Simulink software. They investigated all the main performance parameters within their model. The results showed that their proposed model was able to keep the primary coolant temperature within a safety range for a sufficient time, without the lead freezing or over-heating.

Literature reviews show that no numerical study has been conducted on conjugate pool boiling and condensation in passive heat removal systems. To the best of our knowledge, the main numerical works on this topic were concentrated on either condensation or pool boiling individually, even the phase change was neglected. Furthermore, in all the previous studies, only the horizontal or nearly horizontal direction of the tubes was considered for condensation [1, 19, 30, 35]. Previous studies [9, 10, 36, 37], of the authors showed the potential improvement capacity of the condensation heat transfer coefficient when an inclination angle was imposed on the tube orientation In this paper, conjugate heat transfer, pool boiling outside and condensation inside a smooth tube were investigated numerically. The effects of various parameters, such as steam mass flow rate, steam quality and tube inclination angle on the boiling and condensation heat transfer coefficients, are considered.

2. Mathematical formulation

2.1. Governing equations

In this study, two-fluid multiphase flow formulation is used to simulate pool boiling outside and condensation inside a smooth tube. In the two-fluid multiphase flow approach, governing equations, which consist of mass, momentum and energy equations, can be presented as follows [38]:

$$\frac{\partial}{\partial t}\left(\alpha_i \rho_i\right)+\nabla.\left(\alpha_i \rho_i \vec{u}_i\right)=\sum_{j=1}^{n}\left(\dot{m}_{ji}-\dot{m}_{ij}\right)+S_i \tag{1}$$

$$\frac{\partial}{\partial t}\left(\alpha_i \rho_i \vec{u}_i\right)+\nabla.\left(\alpha_i \rho_i \vec{u}_i \vec{u}_i\right)=-\alpha_i \nabla P+\nabla.\bar{\bar{\tau}}_i+\alpha_i \rho_i \vec{g}+\sum_{j=1}^{n}\left(\dot{m}_{ji}\vec{u}_{ji}-\dot{m}_{ij}\vec{u}_{ij}\right)+\vec{S}_{u,i} \tag{2}$$

$$\frac{\partial}{\partial t}\left(\alpha_i \rho_i h_i\right)+\nabla.\left(\alpha_i \rho_i \vec{u}_i h_i\right)=\alpha_i \frac{\partial P}{\partial t}+\bar{\bar{\tau}}_i : \nabla \vec{u}_i-\nabla.\vec{q}_i+\sum_{j=1}^{n}\left(Q_{ji}+\dot{m}_{ji}h_{ji}-\dot{m}_{ij}h_{ij}\right)+S_{h,i} \tag{3}$$

Where subscripts "*i*" and "*j*" denote the *i*-th and *j*-th phases (which could be liquid (*l*) or vapour (*v*)), ρ is the density, $\dot{m}_{ij}$ is the mass transfer rate between phases, P is pressure, $\vec{u}$ is the velocity vector, $\overline{\overline{\tau}}$ is the stress tensor, t is the time and α is the volume fraction. Additionally, $\vec{g}$ is the gravitational acceleration vector, h is fluid specific enthalpy, $\vec{q}$ is heat flux, h_{ij} is the interphase enthalpy, Q_{ij} is the intensity of heat exchange between the different phases and S, S_u, and S_h are mass, momentum and energy source terms. The heat exchange between phases must comply with the local balance conditions; $Q_{ij} = -Q_{ji}$ and $Q_{ii} = 0$ and can be calculated as:

$$Q_{ij} = h_{interface} A_{interfacial} (T_i - T_j) \tag{4}$$

Where T, $h_{interface}$ and $A_{interfacial}$ are the fluid temperature, interface heat transfer coefficient (see Eq. 32) and interfacial area concentration respectively. . The *i*-th stress tensor, $\overline{\overline{\tau}}$, is also defined as follows [38]:

$$\overline{\overline{\tau}}_i = \alpha_i \mu_i (\nabla \vec{u}_i + \nabla \vec{u}_i^T) + \alpha_i (\lambda_i - \frac{2}{3} \mu_i) \nabla . \vec{u}_i \overline{\overline{I}} \tag{5}$$

Where μ and λ is the viscosity and bulk viscosity of phase *i* respectively.

For modelling the turbulence the two-equation mixture turbulence model, κ-ε, is applied as its suitable performance for the simulation of condensation and boiling in heat removal systems are

already approved [28, 29]. The equations of turbulence energy and dissipation rate are represented as follows [28, 29]:

$$\frac{\partial(\rho_m \kappa)}{\partial t} + \nabla.(\rho_m \vec{u}_m \kappa) = \nabla.[(\mu_{L,m} + \frac{\mu_{t,m}}{\sigma_k})\nabla\kappa] + [\mu_{t,m}(\nabla\vec{u}_m + (\nabla\vec{u}_m)^T) : \nabla.\vec{u}_m] - \rho_m \varepsilon \tag{6}$$

$$\begin{aligned}\frac{\partial(\rho_m \varepsilon)}{\partial t} + \nabla.(\rho_m \vec{u}_m \varepsilon) &= \nabla.[(\mu_{L,m} + \frac{\mu_{t,m}}{\sigma_\varepsilon})\nabla\varepsilon] \\ &+ \frac{\varepsilon}{\kappa}(C_{1\varepsilon}[\mu_{t,m}(\nabla\vec{u}_m + (\nabla\vec{u}_m)^T) : \nabla.\vec{u}_m] - C_{2\varepsilon}\rho_m \varepsilon) + C_{1\varepsilon}C_{3\varepsilon}\frac{\varepsilon}{\kappa}G_b\end{aligned} \tag{7}$$

Where κ and ε, G_b *and* $\vec{u}_m$ are turbulent kinetic energy, turbulent energy dissipation rate, generation of turbulence kinetic energy due to buoyancy and mixture velocity respectively. The turbulent viscosity, μ_t, relates to turbulence energy, κ, and dissipation rate, ε, such that:

$$\mu_{m,t} = C_\mu \frac{\rho_m \kappa^2}{\varepsilon} \tag{8}$$

Where, C_μ, is a function of various parameters and calculated as follows:

$$\begin{aligned}&C_\mu = \frac{1}{A_0 + A_s \frac{kU^*}{\varepsilon}}, U^* = \sqrt{S_{ij}S_{ij} + \tilde{\Omega}_{ij}\tilde{\Omega}_{ij}}, \tilde{\Omega}_{ij} = \Omega_{ij} - 2\varepsilon_{ij}\omega_k \\ &\Omega_{ij} = \bar{\Omega}_{ij} - \varepsilon_{ij}\omega_k\end{aligned} \tag{9}$$

Where, $\bar{\Omega}_{ij}$, the mean rate of rotation tensor in a moving reference frame with an angular velocity of, ω_k. The other constants and parameters are defined as:

$$A_0 = 4.04,\ A_s = \sqrt{6}\cos\varphi,\ \varphi = \frac{1}{3}\cos^{-1}(\sqrt{6}W),\ W = \frac{S_{ij}S_{jk}S_{ki}}{\tilde{S}^3},$$
$$\tilde{S} = \sqrt{S_{ij}S_{ij}},\ S_{ij} = 0.5\left(\frac{\partial u_i}{\partial x_j} + \frac{\partial u_j}{\partial x_i}\right) \tag{10}$$

$$C_{1\varepsilon} = max\left[0.43, \frac{\eta}{\eta+5}\right],\ \eta = S\frac{\kappa}{\varepsilon},\ S = \sqrt{2S_{ij}S_{ij}},\ C_{2\varepsilon} = 1.92,\ C_{3\varepsilon} = tanh\left|\frac{v}{u}\right|,\ \sigma_k = 1.0,\ \sigma_\varepsilon = 1.3 \tag{11}$$

Further details on the constants can be found in [28, 29].

The inter-phase momentum transfer term ($S_{u,i}$) at the liquid-vapour interface accounts for the forces due to viscose drag ($F_{i,Drag}$), lift ($F_{i,lift}$), virtual mass ($F_{i,vm}$), turbulent dispersion ($F_{i,Dispersion}$) and wall lubrication force ($F_{q,wall}$) [39, 40]:

$$S_{u,i} = F_{i,drag} + F_{i,lift} + F_{i,vm} + F_{i,dispersion} + F_{i,wall} \tag{12}$$

The drag force is calculated from the model of Clift *et al.* [41] as follows:

$$F_{i,drag} = \frac{1}{8}C_D\, A_{interfacial}\, \rho_i \left|\vec{u}_j - \vec{u}_i\right|\left(\vec{u}_j - \vec{u}_i\right) \tag{13}$$

$$C_D = max\left[min\left(C_{D,ellipse}, C_{D,cap}\right), C_{D_{Sphere}}\right]$$
$$C_{D_{Sphere}} = \begin{cases} \dfrac{24}{Re} & Re \le 0.01 \\ 24\dfrac{\left(1+0.15\,Re^{0.687}\right)}{Re} & Re > 0.01 \end{cases};\ C_{D,cap} = \frac{8}{3};\ C_{D,ellipse} = \frac{4}{3}\frac{gd_j}{U_t^2}\frac{\left(\rho_i - \rho_j\right)}{\rho_j} \tag{14}$$

$$Re=\frac{\rho_i\left|\vec{u}_j-\vec{u}_i\right|d_j}{\mu_i};\ U_t=\frac{\mu_i}{\rho_i d_j}Mo^{-0.149}\left(J-0.857\right);\ Mo=\frac{\left(\mu_i\right)^4 g\left(\rho_i-\rho_j\right)}{\left(\rho_i\right)^2\sigma^3}$$

$$J=\begin{cases}0.94H^{0.757} & 2<H\le 59.3\\ 3.42H^{0.441} & H>59.3\end{cases};\ H=\frac{4}{3}Eo\,Mo^{-0.149}\left(\frac{\mu_i}{0.0009}\right)^{-0.14} \tag{15}$$

$$Eo=\frac{g\left(\rho_i-\rho_j\right)\left(d_j\right)^2}{\sigma}$$

Where σ is the surface tension, C_D is the drag coefficient, Re is Reynolds number, Mo is Morton number and Eo is Eotvos number. The lift force is calculated using the Tomiyama model [42]:

$$F_{i,lift}=C_L\alpha_j\rho_i\left(\vec{u}_j-\vec{u}_i\right)\times\left(\nabla\times\vec{u}_i\right) \tag{16}$$

$$C_L=\begin{cases}min\left[0.288tanh\left(0.121Re\right),f\left(Eo_d\right)\right] & Eo<4\\ f\left(Eo_d\right)=0.00105Eo_d{}^3-0.0159Eo_d{}^2-0.0204Eo_d+0.474 & 4<Eo<10\\ -0.29 & Eo>10\end{cases} \tag{17}$$

$$Eo_d=\frac{g\left(\rho_i-\rho_j\right)\left(d_i\right)^2}{\sigma}\left(1+0.163Eo^{0.757}\right)^{2/3}$$

To account for wall lubrication and turbulent dispersion forces, the formulations proposed by Antal *et al.* [43] and Burns *et al.* [44] are employed, respectively:

$$F_{i,wall}=C_w\alpha_i\rho_j\left|\vec{u}_j-\vec{u}_i\right|^2\vec{n}_w$$
$$C_w=max\left(0,\frac{C_{w1}}{d_p}+\frac{C_{w2}}{y_w}\right);\ C_{w1}=-0.01;\ C_{w2}=0.05 \tag{18}$$

$$F_{i,dispersion}=C_D\frac{\mu_{j,t}}{\rho_j Sc_j}\left(\frac{\nabla\alpha_j}{\alpha_j}-\frac{\nabla\alpha_i}{\alpha_i}\right) \tag{19}$$

Where *Sc* is Schmidt number. The virtual mass force originates from the acceleration of gas bubbles relative to the continuous liquid phase and can be calculated as:

$$F_{i,vm} = -F_{j,vm} = 0.5\alpha_j \rho_i \left(\frac{D\vec{u}_j}{Dt} - \frac{D\vec{u}_i}{Dt} \right) \tag{20}$$

2.2. Boiling model

To model boiling along the tube wall, the Rensselaer Polytechnic Institute (RPI) nucleate boiling model of Kurul and Podowski [45] is employed. In the RPI model, the total wall heat flux is decomposed into three distinctive elements:

$$\dot{q}_w = \dot{q}_C + \dot{q}_Q + \dot{q}_E \tag{21}$$

Where $\dot{q}_C$ is the convective heat flux, $\dot{q}_Q$ is the quenching heat flux and $\dot{q}_E$ is the evaporative heat flux. The convective heat flux is computed by:

$$\dot{q}_C = h_C \left(T_w - T_l \right) \left(1 - a_b \right) \tag{22}$$

Where h_c is the single-phase heat transfer coefficient, (T_w-T_l) is the wall-liquid temperature difference, and a_b is the part of the wall surface covered by nucleate bubbles and calculated as [46]:

$$a_b = min\left(1, K_{DK}\frac{N_W \pi D_W^2}{4}\right);\quad K_{DK} = 4.8\,exp\left(-\frac{1}{80}\frac{\rho_l C_{p,l}\left(T_{sat}-T_l\right)}{\rho_v h_{lv}}\right) \tag{23}$$

Where T_{sat} is the saturation temperature, h_{lv} is the latent heat of evaporation, D_w is the bubble departure diameter, C_p is the specific heat and N_w is the nucleate site density. The nucleate site density is determined by the correlation of Lemmert and Chawla [47]:

$$N_w = C^n\left(T_w - T_{sat}\right)^n;\ C=210,\ n=1.805 \tag{24}$$

The bubble departure diameter in the RPI model is expressed by:

$$D_w = min\left(0.0014, 0.0006\,exp\left(-\frac{\Delta T_w}{45}\right)\right) \tag{25}$$

As the vapour bubbles periodically detach from the solid wall, a liquid film fills the wall neighbourhood. The average time of the heat transfer rate for this substitute liquid film is expressed by:

$$\dot{q}_Q = \frac{k_l}{\sqrt{\pi\frac{k_l}{\rho_l C_{p,l}}\tau}}\left(T_w - T_l\right) \tag{26}$$

Where k_l is the liquid thermal conductivity and τ is the period of the bubble detachment process, and can be calculated as [48]:

$$\frac{1}{\tau} = \sqrt{\frac{4g\left(\rho_l - \rho_v\right)}{3\rho_l D_w}} \tag{27}$$

Evaporative heat flux is also represented by:

$$\dot{q}_E = \frac{\pi}{6} D_w^3 N_w \rho_v h_{lv} \tag{28}$$

3. Mass transfer mechanisms

In this study, two distinct phase-change mechanisms are considered. The condensation of high-pressure steam occurs inside the tube and, at the same time, the pool boiling of subcooled water liquid takes place outside the tube. Therefore, two separate mass transfer mechanisms are defined.

3.1. Pool boiling outside the tube

The mass transfer rate between the liquid and vapour phases occurs in two distinct regions: near the hot wall and in the bulk liquid. The mass transfer near the hot wall can be calculated by:

$$\dot{m}_{boiling,1} = \frac{\dot{q}_E}{h_{lv} + C_{p,l}\left(T_{sat} - T_l\right)} \tag{29}$$

The mass transfer rate at the bulk saturated liquid region can be determined as:

$$\dot{m}_{boiling,2} = \frac{\dot{q}_l + \dot{q}_v}{h_{lv}} \tag{30}$$

$$\dot{q}_l = \frac{k_l Nu}{D_w}\left(T_{sat} - T_l\right);\ \dot{q}_v = \frac{\alpha_v \rho_v C_{p,v}}{\delta t}\left(T_{sat} - T_v\right) \tag{31}$$

Where δt denotes the time scale set to 0.05 [28, 29]. The correlation of Ranz and Marshall [49] is used for computing the Nu number and corresponding Q at the interface as:

$$Nu_l = 2 + 0.6\, Re^{1/2}\, Pr^{1/3} \tag{32}$$

$$Q_{lv} = Nu \frac{k_l}{d_l} A_{interfacial}(T_v - T_l) \tag{33}$$

Where Pr is the Prandtl numbers. Moreover the interfacial area concentration, $A_{interfacial}$, can be calculated as follows [28, 29]:

$$A_{interfacial} = min(1, 0.57, \pi D_w{}^2 N_w) \tag{34}$$

3.2. Condensation inside the tube

In this study, the direct heat balance equation across the interface is used to calculate the condensation rate. The heat balance at the liquid-vapour interface is defined as [50]:

$$\dot{m}_{condnesation} = \frac{k_v \nabla T_v \nabla \alpha_v - k_l \nabla T_l \nabla \alpha_l}{h_{lv}} \tag{35}$$

Further details on the derivation of the above equation can be found in Carey [50] and it is not further discussed here for brevity.

4. Numerical method

The numerical simulation of pool boiling on smooth, inclined tubes was performed on an ANSYS Fluent 17.1 commercial CFD package. A phase-coupled SIMPLE method was employed to handle the pressure velocity coupling. The convective terms in governing equations were approximated by a second-order upwind scheme and the gradient of all the flow variables was calculated using the least-square cell-based method. Moreover, the volume fraction equation was solved by modifying the HRIC scheme. Transient simulations were progressed in time by a global courant number of 0.1, which guaranteed the stability of the numerical approach. Finally, the convergence criterion was set at 10^{-5} for all the flow equations.

4.1. Assumptions

The following assumptions are considered for the present numerical simulation:

1. The flow field is three-dimensional, transient and turbulent.
2. The properties of each phase are assumed to be constant under the specified operating condition.
3. The interface temperature is assumed to be at the saturation temperature.
4. No-slip condition is considered for all the walls within the computational domain.
5. The contact angle between the liquid and vapour phases is considered to be 80° [12].
6. A time step size of 10^{-5} s is chosen for the simulations.

7. The simulations continued until the changes in the condensation and pool boiling heat transfer coefficients are below 2%. The corresponding time for this criterion is t = 240 s for all cases.

4.2. Boundary and initial conditions

Fig. 1 shows the physical domain and the relevant computational grid. The following boundary conditions are set for the simulations:

1. Tube inlet: Saturated steam at the fixed temperature of 250 °C with the specified quality and mass flow rate enters the tube.
2. Tube wall: The no-slip condition is set for the tube wall. Moreover, the thickness of the tube wall is 3 mm. As the conjugate heat transfer is considered for the tube wall, there is no need to specify any temperature of heat flux boundary condition.
3. Tube outlet: The gauge pressure at the outlet of the tube is set to 0.
4. Pool walls: All walls of the pool are adiabatic with no-slip condition.
5. Pool opening: The upper part of the pool is open to attain saturation pressure.

At the start of each simulation, the pool is considered to be filled with water liquid with a temperature of 25 °C and at atmospheric pressure (saturation temperature of 100 °C). Moreover, the tube is filled with the vapour at the saturation temperature of 250 °C.

5. Results and discussion

As discussed previously, in this study, two phase-change phenomena are considered simultaneously. The physical domain of the present numerical simulation is depicted in Fig. 1. The

computational domain consists of a pool with the size of 300 × 300 × 500 mm and a smooth steel tube with inner and outer diameters of 19 mm and 25 mm respectively. The selected computational domain is from the recent experimental work of Nie *et al.* [26]. The experimental work was only conducted on a horizontal tube with a large steam mass flow rate and focused on condensation and not pool boiling. In the present study, the effect of the inclination angle, steam mass flow rate and quality is taken into account. The simulation cases are presented in Table 1.

5.1. Validation of the numerical method

To obtain the optimum mesh size, a grid study is performed. Fig. 2 shows the variations of condensation and pool boiling heat transfer coefficients for G = 200 kg/m^{2}s and x_{in} = 0.2 for different grid sizes. As can be seen in this figure, the results do not change considerably with a grid size smaller than 892 112 cells. Therefore, a grid size of 892 112 cells is utilized for the present numerical simulations. It is worth mentioning that the boundary layer with 10 rows and an aspect ratio of 1.2 is used to attain the y^+ values between 1.3 to 3.0 at both sides of the tube.

Fig. 3 shows the simulated results for the condensation heat transfer coefficient and pressure drop for a steam mass flow rate of 400 kg/m^{2}s, pool temperature of 25 °C and tube side saturation temperature of 250 °C. The results clearly show that the present numerical method can well predict the flow and temperature field within the computational domain. To evaluate the performance of the present numerical simulation for the conjugate heat transfer along the tube thickness, a comparison is made between the present study for the inner and outer wall temperatures, and the experimental data. Fig. 4 shows the variation of the inner and outer wall temperatures for a steam mass flow rate of 400 kg/m^{2}s, pool temperature of 25 °C and tube side saturation temperature of

250 °C. As can be seen in this figure, the calculated results are in good agreement with the experimental data.

5.2. Description of phase-change mechanisms

As discussed previously, in this study, both the condensation and pool boiling phenomena are considered within the simulations. In this section, a detailed explanation of such phase changes is presented. Figs. 5-7 show the contours of the liquid volume fraction inside tube, inner tube surface temperature and vapour volume fraction within the pool for the horizontal tube orientation at G = 400 kg/m^{2}s and various inlet vapour qualities respectively (The contours are illustrated only for the heating section of the tube).

It is clear that, due to the higher density of the liquid phase, the value of the liquid volume fraction is higher at the bottom of the tube (Fig. 5). But it should be noted that the variations of vapour volume fraction from the top side down to the bottom side of the tube is not significant. It is due to the fact that, at the specified steam mass flux and short length of the tube, the flow regime is almost annular. However, with an increase in inlet vapour quality, the changes in vapour volume fraction diminish gradually, which means that the liquid film thickness is circumferentially equal. It can also be deduced from the contours that the liquid film thickness decreases with the increase of vapour quality, which results in the increase of the condensation heat transfer coefficient. This conclusion is used in Sec. 5.3.

In Fig. 6, the contours of outside tube temperature is depicted. The temperature of the tube wall decreases along the tube due to condensation phenomena. However due to the high speed of the

inlet steam and short length of the tube the temperature does not fall significantly. The contours also show that with an increase of inlet vapour mass fraction the overall temperature of the tube surface increases. It can be attributed that with the increase of inlet vapour quality the liquid film thickness decreases, which corresponds to the higher temperature on the tube surface. The tube temperature also varies circumferentially around the tube, because the liquid film thickness is higher at the bottom side of the tube. This agglomeration of the liquid film at the bottom of the tube causes the higher heat resistance toward the heat flux and lower condensation mass transfer rate as well. It should be noted that this difference in the temperature is not very clear, particularly in higher inlet vapour mass fraction, because the flow regime is almost annular inside the tube.

Fig. 7 shows the contours of the vapour volume fraction for $\theta = 0$ (horizontal orientation of the tube) at $G = 400$ kg/m^{2}s and various inlet vapour qualities. The figure shows that, with an increase in inlet vapour quality, the condensation mass transfer rate increases and hence the corresponding heat flux to the pool side increases. Therefore, the produced vapour in the pool side increases due to a higher heat transfer rate and tube temperature. As the Eulerian-Eulerian multiphase flow approach is used for the present numerical simulations, the vapour phase can be distinguished by a fog of vapour phase around the tube rather than separate bubbles which are form by nucleate boiling phenomenon.

5.3. Condensation inside tube

Fig. 8 shows the variations in the condensation heat transfer coefficient for different tube inclinations and steam mass flow rates. The plot clearly shows that the condensation heat transfer coefficients increase with an increase in the steam mass flow rate and inlet steam quality. With an

increase in inlet vapour quality, the thickness of the liquid film near the tube wall, which acts as an obstacle to heat transfer decreases and as a results the condensation heat transfer coefficient increases. The increase in the steam mass flux increases the convection effect inside the tube which consequently causes the increase in condensation heat transfer coefficient. The results also show that the inclination has no significant effect at these high steam mass flow rates in which the flow regimes are almost annular. However, the graphs show some partial maxima at the negative inclination angles. The simulated results are compatible with the experimental data of Wang and Du [51], in which they concluded that there was no particular trend for the variations in the condensation heat transfer of steam at a tube inclination angle when the flow regime is almost annular. Although the previous results from the authors [8-10, 36] showed the existence of an optimum point between θ = -30° and θ = -15° for the condensation of R134a inside a smooth tube with a constant heat flux, in the present numerical simulation, the heat flux changes significantly with the tube orientation due to the effect of pool boiling outside the tube.

Fig. 9 shows the variations in the condensation heat transfer coefficient with respect to tube inclination angle and inlet steam quality. As discussed previously, the condensation heat transfer coefficient increases with an increase in the inlet steam quality due to a decrease in liquid film thickness, which acts as a resistance to the heat flux. The results also show that the increase of steam mass flux increases the condensation heat transfer coefficient due to increase of convection effect inside the tube.

5.4. Pool boiling outside the tube

Fig. 10 shows the variations of the boiling heat transfer coefficient with the inlet steam quality, inclination angle and steam mass flow rate. The plots show that as the inlet steam quality and steam mass flow rate increase, the pool boiling heat transfer coefficient also increases, but this increase varies at different inclination angles. Generally the results show that the boiling heat transfer coefficient is not very sensitive to the tube inclination angle. This trend is against the experimental data of Kang [13], in which the boiling heat transfer coefficient had a maximum and decreased with inclination angle. However, it is important to notice that in this study, as well as in many other previous studies on the phenomenon of nucleate pool boiling the heat flux on the tube surface were constant for all inclination angles. As the inclination angles changed the heat flux produced by the condensation also changed, therefore it can affect the pool boiling heat transfer coefficients. The results presented in Figs. 8 and 9 show that the lowest heat transfer coefficient occurs at the horizontal tube orientation. This case corresponds to the highest heat transfer coefficient for the pool boiling. Therefore, there is an optimum between these two heat transfer coefficients. It can be concluded that the decrease in the pool boiling heat transfer coefficient when an inclination angle is imposed is compensated by the increase in the condensation heat transfer coefficient inside the tube. Therefore, there is a need to use the definition of the total heat transfer coefficient to assess the overall performance of such system (Sec. 5.5). Furthermore, maximum pool boiling heat transfer coefficients occur between θ = -60° and θ = -30°, and between θ = +30° and θ = +60°, in which the condensation heat transfer coefficient seems to be higher.

5.5. Total heat transfer coefficient

Previous studies of pool boiling phenomena regarding the inclination effect showed that, with an increase in tube orientation angle, the pool boiling heat transfer coefficient decreases [13]. But, as

discussed previously, the inclination of the tube causes an increase in the inside heat transfer coefficient. Therefore, we utilize the definition of total (overall) heat transfer coefficient, U_{total}, to investigate the effect of inclination angle more accurately. The total heat transfer coefficient can be calculated as:

$$\frac{1}{(UA)_{total}} = \frac{1}{h_{condenation}(2\pi r_i L)} + \frac{Ln(r_o / r_i)}{2\pi Lk} + \frac{1}{h_{pool\,boiling}(2\pi r_o L)} \tag{36}$$

Where r_i, r_o and L are the tube inner radius, outer radius and length respectively. Moreover, k, is the tube shell thermal conductivity.

Fig. 11 shows the variations of total heat transfer coefficient with respect to the steam mass flux at different tube inclination angles. The plots show that the total heat transfer coefficient increase with the increase of steam mass flux, but this increase is not considerable at higher steam mass fluxes. One important result from this figure is that all the plots show a partial minimum point at a horizontal tube orientation. This may be due to the fact that, at a horizontal orientation, the effect of the gravity force along the flow direction vanishes and the thickness of the liquid film increases. Such trend can also be seen in the previous experimental of Meyer and his co-workers [9, 10, 37], in which the heat transfer coefficients were larger for upward and downward flow direction compared to the horizontal case. It should be noted that such cases are observed for high mass flow rates and vapour qualities, which happen in the present study as well. Also, in all the plots, the total heat transfer coefficient is at its maximum or partially maximum at the inclination angle between θ = -60° and θ = -30°.

Fig. 12 show the effect of the inlet steam mass fraction on the variations of the total heat transfer coefficient at different tube orientations. The total heat transfer coefficient increases with an increase in the steam mass flow rate and inlet steam quality. The increase in the total heat transfer coefficient with respect to the inlet steam mass fraction is more considerable at lower steam mass fractions. Here again, there is no clear trend can be observed for the variations of the total heat transfer coefficient with respect to the tube inclination angle, except for the particular case of $\theta = 0$, in which a partial minimum can be seen.

5.6. Pressure drop

Fig. 13 shows the variations in pressure drop along the tube for different steam qualities, steam mass flow rates and inclination angles. The results show that the pressure drop along the tube increases with an increase of steam mass flux due to the increase of the shear stress and convection effect. Furthermore it can be seen from this figure that the pressure drop along the tube increase with an increase of steam quality. This can be due to the fact that the pressure drop along the tube increases with an increase in inlet steam quality due to the higher kinematic viscosity of the vapour phase, compared to that of the liquid phase. The plots also show that the tube orientation has a significant effect on the pressure drop along the tube. The effect of inclination angle on the pressure drop is more significant at lower steam mass fluxes. It can be attributed to the fact that at higher steam mass fluxes the shear stress force is dominant compared to the gravitational force. It is interesting to note that in some cases, particularly at low steam mass fluxes and for a downward flow direction, that the pressure drop along the tube becomes negative. In downward flow directions the pressure increases when compared to the vertical orientation. This is contrary regardless of the tube orientations as the pressure drop decreases along the tube due to the friction

and momentum losses. When the steam mass flux and quality are low, the effect of height excels the effect of friction and causes a negative pressure drop along the tube.

6. Conclusion

Conjugate condensation and pool boiling phenomena at both sides of a smooth tube were investigated in the present numerical study. The effect of various parameters, such as tube inclination angle, inlet steam quality and steam mass flow rate, on the total heat transfer coefficient was considered. The three-dimensional, unsteady and turbulent flow field governing equations, as well as phase-change source terms, is solved using the ANSYS FLUENT 17.1 commercial package software. Moreover, the results showed good agreement with the available experimental data. Within the numerical simulation the following conclusions are made:

1. It was found that the condensation heat transfer coefficient increases with an increase in the inlet steam quality and steam mass flow rate.
2. A particular trend for the effect of tube orientation on the total heat transfer coefficient was not found. This result was in compatible with previous experimental studies.
3. The pressure drop along the tube increased with increase of steam mass flow rate and quality.
4. The results showed that there is a partial maximum point for the total heat transfer coefficient at an inclination angle between θ = -60° and θ = -30°.

Based on the abovementioned conclusions, it is recommended to designers to impose an appropriate inclination angle of 60° < θ < -30° to achieve higher heat transfer rates without significant additional costs. Further studies in these field should consider the effect of different

saturation temperatures either in the pool or inside the tube. A proper set of saturation temperatures may lead to higher system heat transfer rates.

References

[1] B.Y. Yun, H.C. NO, C.W. Shin, Modeling of high pressure steam condensation in inclined horizontal tubes of PAFS in APR+, J. NUC. SCI. TECHNOL., 53 (2016) 1353-1365.
[2] M.M. Shah, A general correlation for heat transfer during film condensation inside pipes, Int. J. Heat Mass Transfer, 22 (1979) 547-556.
[3] L. Liebenberg, J.P. Meyer, A review of flow pattern-based predictive correlations during refrigerant condensation in horizontally smooth and enhanced tubes, Heat Transf. Eng., 29 (2008) 3-19.
[4] M.B.O. Didi, N. Kattan, J.R. Thome, Prediction of two-phase pressure gradients of refrigerants in horizontal tubes, Int. J. Refrig., 25 (2002) 935-947.
[5] A. Cavallini, D.D. Col, L. Doretti, M. Matkovic, L. Rossetto, C. Zilio, G. Censi, Condensation in horizontal smooth tubes: a new heat transfer model for heat exchanger design, Heat Transfer Eng. , 27 (2006) 31-38.
[6] G. Caruso, D.V.D. Maio, A. Naviglio, Condensation heat transfer coefficient with non-condensable gases inside near horizontal tubes, Desalination, 309 (2013) 247-253.
[7] M.M. Shah, Prediction of heat transfer during condensation in inclined plain tubes, Appl. Therm. Eng., 94 (2016) 82-89.
[8] S. Lips, J.P. Meyer, Effect of Gravity Forces on Heat Transfer and Pressure Drop During Condensation of R134a, Microgravity Sci. Technol. , 24 (2012) 157-164.
[9] S. Lips, J.P. Meyer, Experimental study of convective condensation in an inclined smooth tube. Part II: Inclination effect on pressure drops and void fractions, Int. J. Heat Mass Transfer, 55 (2012) 405-412.
[10] S. Lips, J.P. Meyer, Experimental study of convective condensation in an inclined smooth tube. Part I: Inclination effect on flow pattern and heat transfer coefficient, Int. J. Heat Mass Transfer, 55 (2012) 395-404.
[11] L. Aprin, P. Mercier, L. Tadrist, Local heat transfer analysis for boiling of hydrocarbons in complex geometries: A new approach for heat transfer prediction in staggered tube bundle, Int. J. Heat Mass Transfer, 54 (2011) 4203-4219.
[12] J. Barber, D. Brutin, K. Sefiane, L. Tadrist, Bubble confinement in flow boiling of FC-72 in a rectangular microchannel of high aspect ratio, Exp. Therm. Fluid Sci., 34 (2010) 1375-1388.
[13] M.G. Kang, Pool boiling heat transfer from an inclined tube bundle Int. J. Heat Mass Transfer, 101 (2016) 445-451.
[14] S. Kumar, B. Mohanty, S.G. Gupta, Boiling heat transfer from a vertical row of horizontal tubes, Int. J. Heat Mass Transfer, 45 (2002) 3857-3864.
[15] G. Ribatski, J.M.S. Jabardo, E.F.d. Silva, Modeling and experimental study of nucleate boiling on a vertical array of horizontal plain tubes, Exp. Therm. Fluid Sci., 32 (2008) 1530-1537.
[16] E. Gorgy, S. Eckels, Local heat transfer coefficient for pool boiling of R-134a and R-123 on smooth and enhanced tubes, Int J. Heat Mass Transfer, 55 (2012) 3021-3028.
[17] K. Krasowski, J. Cieslinski, Nucleate pool boiling heat transfer from small horizontal smooth tube bundles, Transactions of the Institute of Fluid-Flow Machinery, 123 (2011) 85-98.
[18] N. Minocha, J.B. Joshi, A.K. Nayak, P.K. Vijayan, Numerical investigation of three-dimensional natural circulation phenomenon in passive safety systems for decay heat removal in large pools, Int. J. Heat Mass Transfer, 81 (2015) 659-680.

[19] X. Wu, C. Yan, Z. Meng, K. Chen, S. Song, Z. Yang, J. Yu, Numerical analysis of the passive heat removal system for molten salt reactor at steady state, Appl. Therm. Eng., 102 (2016) 1337-1344.
[20] Y. Zhang, D. Lu, Z. Du, X. Fu, G. Wu, Numerical and experimental investigation on the transient heat transfer characteristics of C-shape rod bundles used in Passive Residual Heat Removal Heat Exchangers, Ann. Nucl. Energy, 83 (2015) 147-160.
[21] A.A. Ganguli, M.J. Sathe, A.B. Pandit, J.B. Joshi, P.K. Vijayan, Hydrodynamics and heat transfer characteristics of passive decay heat removal systems: CFD simulations and experimental measurements, Chem. Eng. Sci., 65 (2010) 3457-3473.
[22] C.W. Shin, H.C. NO, B.Y. Yun, B.G. Jeon, The experimental investigation of tube's diameter and inclination angle in a separate effect PAFS test facility for APR+, Int. J. Heat Mass Transfer, 86 (2015) 914-922.
[23] X. Wu, C. Yan, Z.Meng, K. Chen, S. Song, Z. Yang, J. Yu, Investigation of Characteristics of Passive Heat Removal System Based on the Assembled Heat Transfer Tube, Nuc. Eng. Tech., 48 (2010) 1321-1329.
[24] J. Wu, Q. Bi, C. Zhou, Experimental study on circulation characteristics of secondary passive heat removal system for Chinese pressurized water reactor, Appl. Therm. Eng., 77 (2015) 106-112.
[25] K. Chen, C. Yan, Z. Meng, X.Wu, S.Song, Z.Yang, J.Yu, Experimental analysis on passive residual heat removal in molten salt reactor using single cooling thimble test system, Energy, 112 (2016) 1049-1059.
[26] Z. Nie, Q. Bi, S. Lei, H. Lv, Y. Guo, Experimental study on condensation of high-pressure steam in a horizontal tube with pool boiling outside, Int. J. Heat Mass Transfer, 108 (2017) 2523-2533.
[27] W.W. Akers, H.A. Deans, O.K. Crosser, Condensing heat transfer within horizontal tubes, J. Chem. Eng. Prog. Symp. Ser., 55 (1959) 171-176.
[28] N. Minocha, J.B. Joshi, A.K. Nayak, P.K. Vijayan, 3D CFD simulations to study the effect of inclination of condenser tube on natural convection and thermal stratification in a passive decay heat removal system, Nuc. Eng. Des., 305 (2016) 582-603.
[29] N. Minocha, J.B. Joshi, A.K. Nayak, P.K. Vijayan, 3D CFD simulation of passive decay heat removal system under boiling conditions: Role of bubble sliding motion on inclined heated tubes, Chem. Eng. Sci., 145 (2016) 245-265.
[30] K.D. Dijo, R.P. Mangarjuna, B.K. Nashine, P. Selvaraj, P. Chellapandi, Numerical simulation of passive heat removal under severe core meltdown scenario in a sodium cooled fast reactor, Nuc. Eng. Des., 291 (2015) 188-203.
[31] T.C. Hung, V.K. Dhir, J.C. Chang, S.K. Wang, CFD modeling and thermal-hydraulic analysis for the passive decay heat removal of a sodium-cooled fast reactor, Nuc. Eng. Des., 241 (2011) 425-432.
[32] H. Mochizuki, T. Yano, A passive decay-heat removal system for an ABWR based on air cooling, Nuc. Eng. Des., 311 (2017) 35-42.
[33] H. Ayhan, C.N. Sökmen, Investigation of passive residual heat removal system for VVERs: Effects of finned type heat exchanger tubes, Appl. Therm. Eng. , 108 (2016) 466-474.
[34] L. Damiani, P. Giribone, R. Revetria, A.P. Prato, A passive decay heat removal system for the lead cooled fast reactor demonstrator "Alfred", Prog. Nuc. Energy, 83 (2015) 294-304.
[35] E. Krepper, M. Beyer, Experimental and numerical investigations of natural circulation phenomena in passive safety systems for decay heat removal in large pools, Nuc. Eng. Des., 240 (2010) 3170-3177.
[36] J.P. Meyer, J. Dirker, A.O. Adelaja, Condensation heat transfer in smooth inclined tubes for R134a at different saturation temperatures, Int. J. Heat Mass Transfer, 70 (2014) 515-525.
[37] S.P. Olivier, J.P. Meyer, M.D. Paepe, K.D. Kerpel, The influence of inclination angle on void fraction and heat transfer during condensation inside a smooth tube, Int. J. Multi. Flow, 80 (2016) 1-14.
[38] L. Kataoka, A. Serizawa, Basic equations of turbulence in gas-liquid two-phase flow, Int. J. Multi. Flow, 15 (1989) 843-855.

[39] W. Yao, C. Morel, Volumetric area prediction in upward bubbly two-phase flow, Int. J. Heat Mass Transfer, 47 (2004) 307-328.
[40] A. Ahmadpour, S.M.A.N.R. Abadi, R. Kouhikamali, Numerical simulation of two-phase gas–liquid flow through gradual expansions/contractions, Int. J. Multi. Flow (79) (2016) 31-49.
[41] R. Clift, J.R. Grace, M.E. Weber, Bubbles, Drops and Particles, Academic Press, (1978).
[42] A. Tomiyama, Struggle with computational bubble dynamics, Third International Conference on Multiphase Flow, Lyon France, June (1998) 8-12.
[43] S.P. Antal, R.T. Lahey, J.E. Flaherty, Analysis of phase distribution in fully developed laminar bubbly two-phase flow, Int. J. Multi. Flow, 17 (1991) 635-652.
[44] A.D. Burns, T. Frank, I. Hamill, J.M. Shi, The Favre averaged drag model for turbulent dispersion in Eulerian multi-phase flows, Fifth International Conference on Multiphase Flow, ICMF-2004, Yokohama, Japan, (2004).
[45] N. Kurul, M.Z. Podowski, On the modeling of multidimensional effects in boiling channels, Proceedings of the 27th National Heat Transfer Conference, Minneapolis, Minnesota, USA, (1991).
[46] V.H.D. Valle, D.B.R. Kenning, Sub-cooled flow boiling at high heat flux, Int. J. Heat Mass Transfer, 28 (1985) 1907-1920.
[47] M. Lemmert, L.M. Chawla, Influence of flow velocity on surface boiling heat transfer coefficient in Heat Transfer in Boiling, Academic Press and Hemisphere, (1977).
[48] R. Cole, A Photographic Study of Pool Boiling in the Region of the Critical Heat Flux, AIChE J., 6 (1960) 533-542.
[49] W.E. Ranz, W.R. Marshall, Jr. Vaporation from Drops, Part I, Chem. Eng. Prog., 48 (1952) 141-146.
[50] V.P. Carey, Liquid-Vapor Phase-Change Phenomena, 2nd. ed. Taylor and Francis Group, LLC, New York, USA, (2008).
[51] B. Wang, X. Du, Study on laminar film-wise condensation for vapor flow in an inclined small/mini-diameter tube, Int. J. Heat Mass Transfer, 43 (2000) 1859-1868.

List of figure captions

Fig. 1. Computational domain.

Fig. 2. Effect of grid size on: (a) condensation heat transfer coefficient; and (b) static pressure drop for G = 200 kg/m^{2}s and x_{in} = 0.2.

Fig. 3. Comparison between present numerical results and experimental data of Nie *et al.* [26]: (a) condensation heat transfer coefficient; and (b) pressure drop at G = 400 kg/m^{2}s and θ = 0.

Fig. 4. Comparison between present numerical results and experimental data of Nie *et al.* [26]: (a) inner tube wall temperature; and (b) outer tube wall temperature at G = 400 kg/m^{2}s and θ = 0.

Fig. 5. Contours of liquid volume fraction inside the tube for the horizontal tube orientation for G = 400 kg/m^{2}s: (a) x_{in} = 0.2, (b) x_{in} = 0.4, (c) x_{in} = 0.6, (d) x_{in} = 0.8.

Fig. 6. Contours of tube inner surface temperature, in Kelvin, for the horizontal tube orientation at G = 400 kg/m^{2}s: (a) x_{in} = 0.2; (b) x_{in} = 0.4; and (c) x_{in} = 0.6, (d) x_{in} = 0.8.

Fig. 7. Contours of tube vapour volume fraction within the pool for the horizontal tube orientation at G = 400 kg/m^{2}s: (a) x_{in} = 0.2; (b) x_{in} = 0.4; and (c) x_{in} = 0.6, (d) x_{in} = 0.8.

Fig. 8. Variations of condensation heat transfer coefficient for different tube inclinations and steam mass flow rates: (a) x_{in} = 0.2; (b) x_{in} = 0.4; (c) x_{in} = 0.6; and (d) x_{in} = 0.8.

Fig. 9. Variations of condensation heat transfer coefficient with respect to tube inclination angle and inlet steam qualities: (a) G = 100 kg/m^{2}s; (b) G = 200 kg/m^{2}s; and (c) G = 400 kg/m^{2}s.

Fig. 10. Variations of boiling heat transfer coefficient with inlet steam quality and inclination angle: (a) G = 100 kg/m^{2}s; (b) G = 200 kg/m^{2}s; and (c) G = 400 kg/m^{2}s.

Fig. 11. Variations of total heat transfer coefficient with respect to steam mass flow rate and tube orientation: (a) x_{in} = 0.2; (b) x_{in} = 0.4; (c) x_{in} = 0.6; and (d) x_{in} = 0.8.

Fig. 12. Variations of total heat transfer coefficient with respect to inlet steam quality and tube orientation: (a) G = 100 kg/m^{2}s; (b) G = 200 kg/m^{2}s; and (c) G = 400 kg/m^{2}s.

Fig. 13. Variations of pressure drop along the tube for different steam mass flow rates and inclination angles: (a) x_{in} = 0.2; (b) x_{in} = 0.4; (c) x_{in} = 0.6; and (d) x_{in} = 0.8.

List of table captions

Table 1. Different operating conditions considered in the simulations.

Figures:

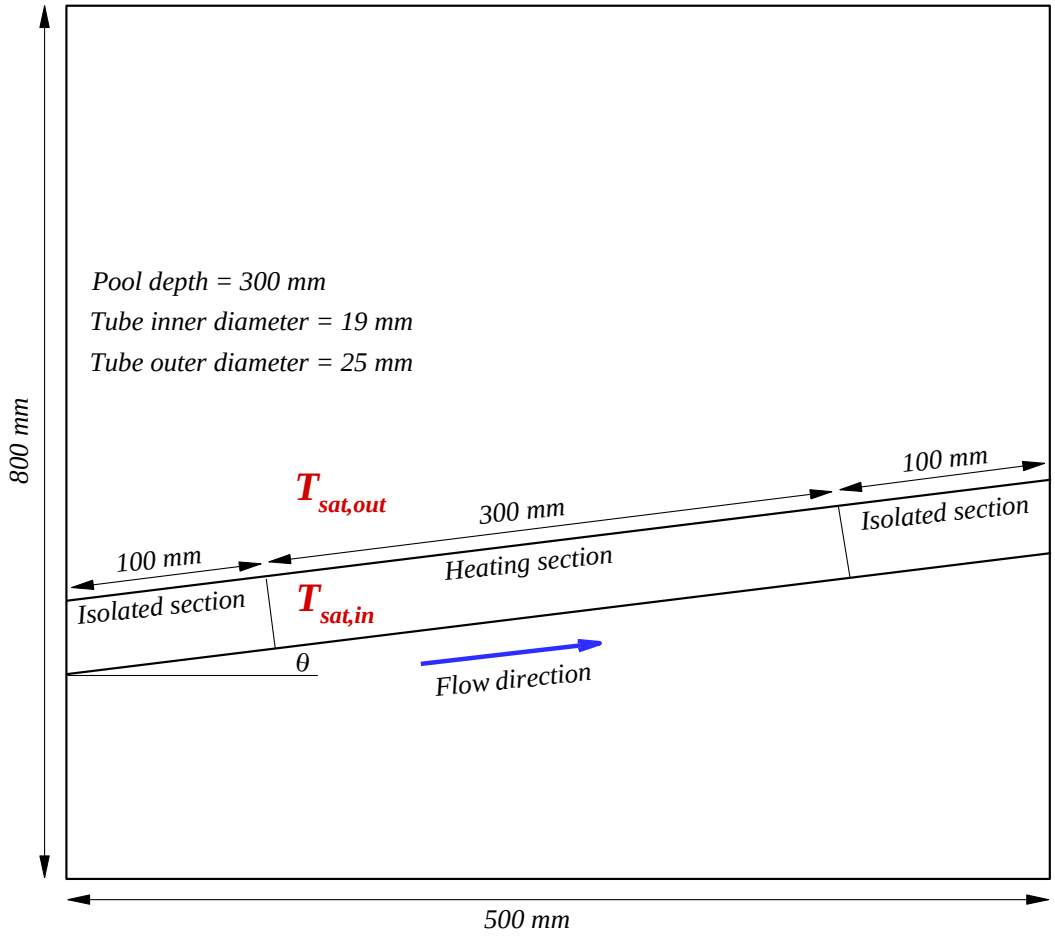

Fig. 1

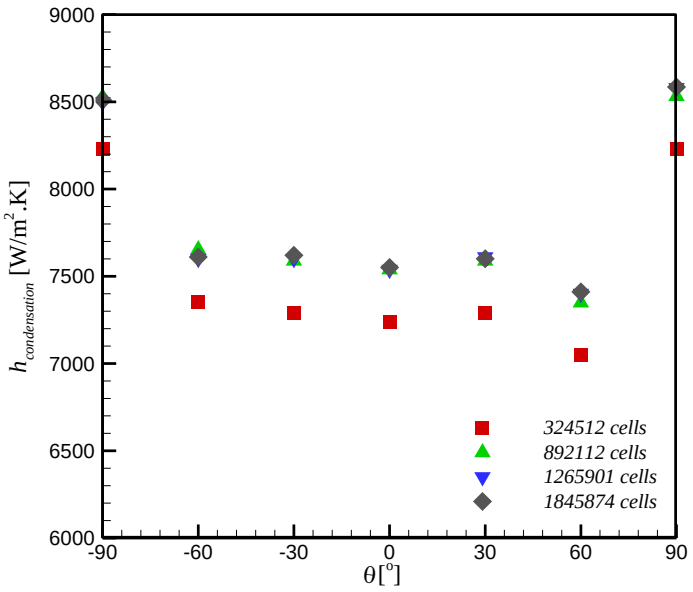
9000
8500
8000
7500
7000
6500
6000
$h_{condensation}$ [W/m^2.K]
-90
-60
-30
0
30
60
90
θ[°]
324512 cells
892112 cells
1265901 cells
1845874 cells

(a)

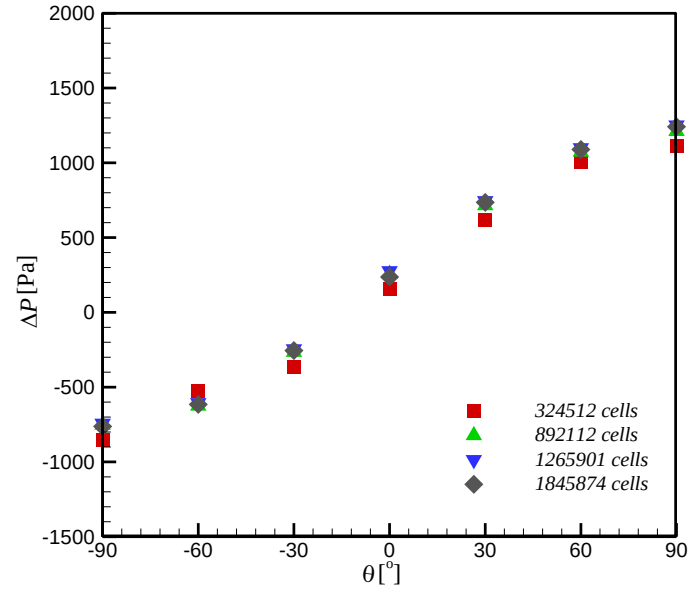
2000
1500
1000
500
0
-500
-1000
-1500
ΔP [Pa]
-90
-60
-30
0
30
60
90
θ[°]
324512 cells
892112 cells
1265901 cells
1845874 cells

(b)

Fig. 2

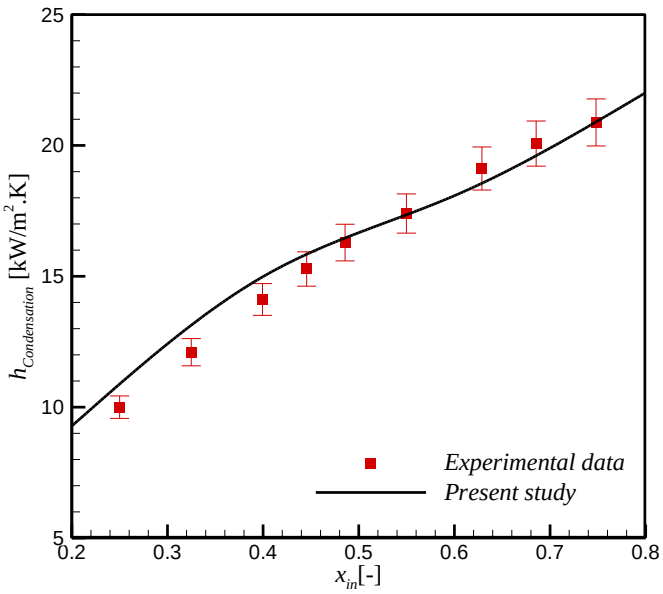
25
20
15
10
5
0.2
0.3
0.4
0.5
0.6
0.7
0.8
$h_{Condensation}$ [kW/m^2.K]
x_{in}[-]
Experimental data
Present study

(a)

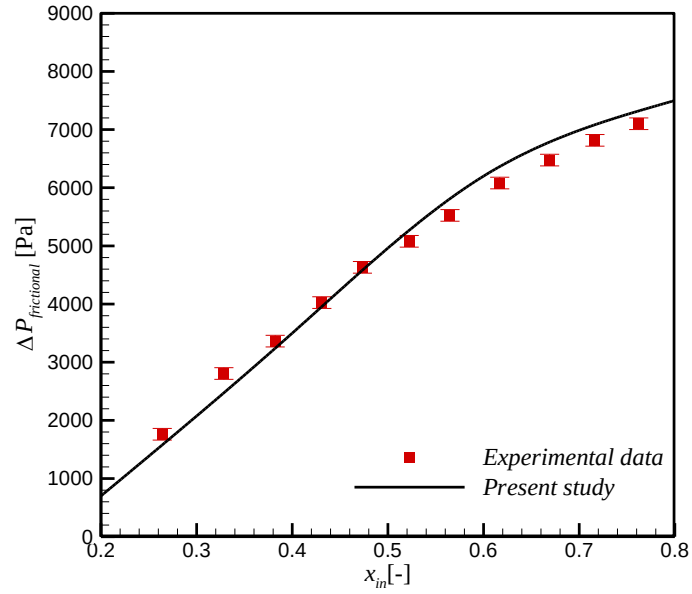
9000
8000
7000
6000
5000
4000
3000
2000
1000
0
0.2
0.3
0.4
0.5
0.6
0.7
0.8
$\Delta P_{frictional}$ [Pa]
x_{in}[-]
Experimental data
Present study

(b)

Fig. 3

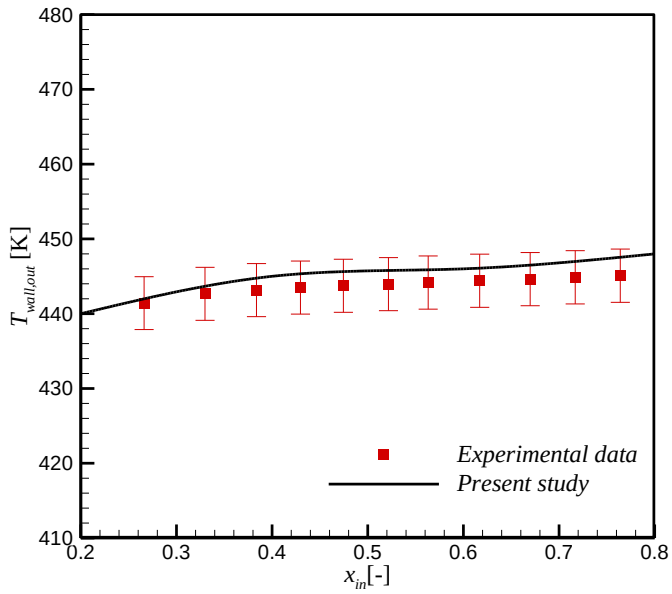
480
470
460
450
440
430
420
410
0.2
0.3
0.4
0.5
0.6
0.7
0.8
$T_{wall,out}$ [K]
x_{in}[-]
Experimental data
Present study

(a)

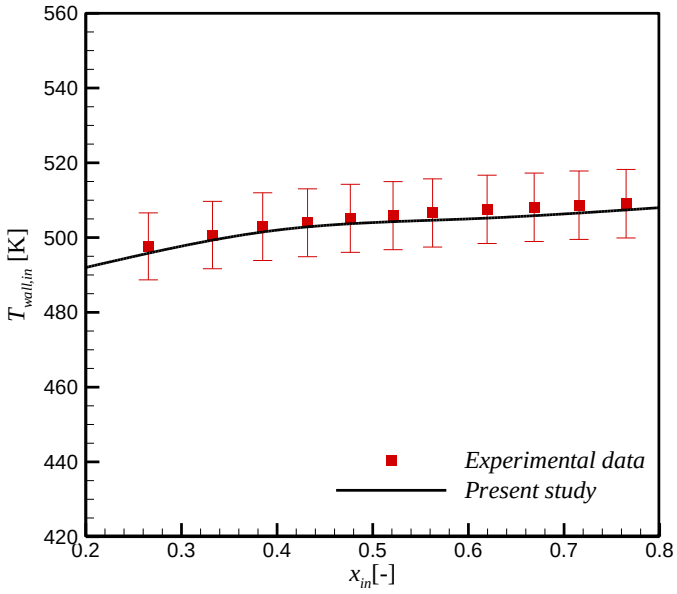
560
540
520
500
480
460
440
420
0.2
0.3
0.4
0.5
0.6
0.7
0.8
$T_{wall,in}$ [K]
x_{in}[-]
Experimental data
Present study

(b)

Fig. 4

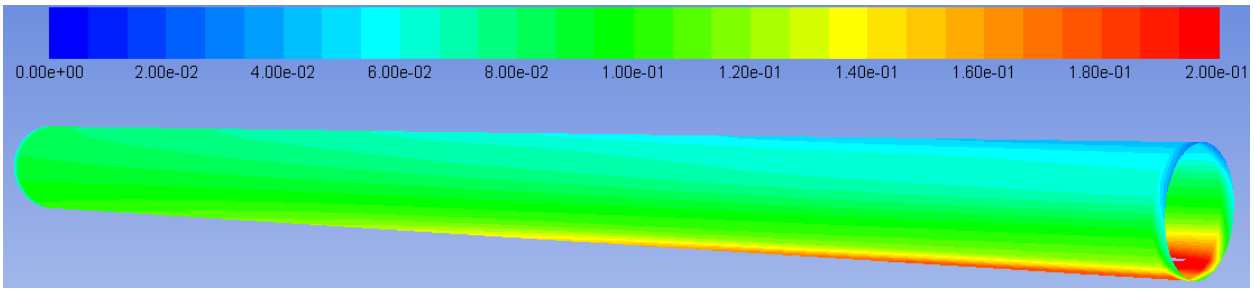

(a) x_{in} = 0.2

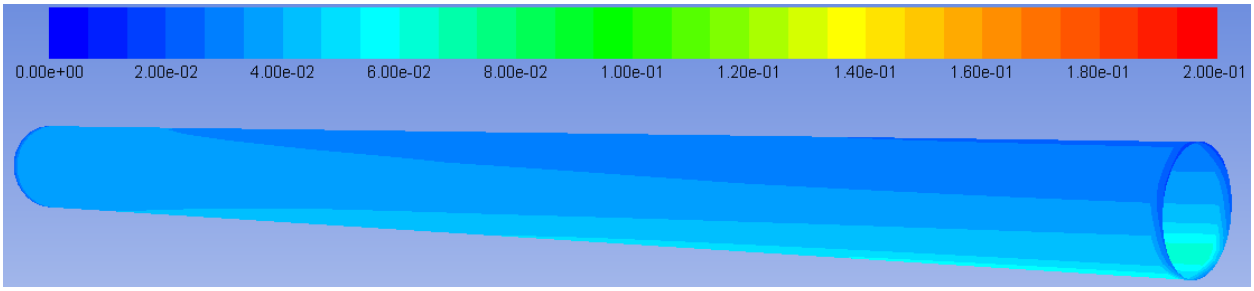

(b) x_{in} = 0.4

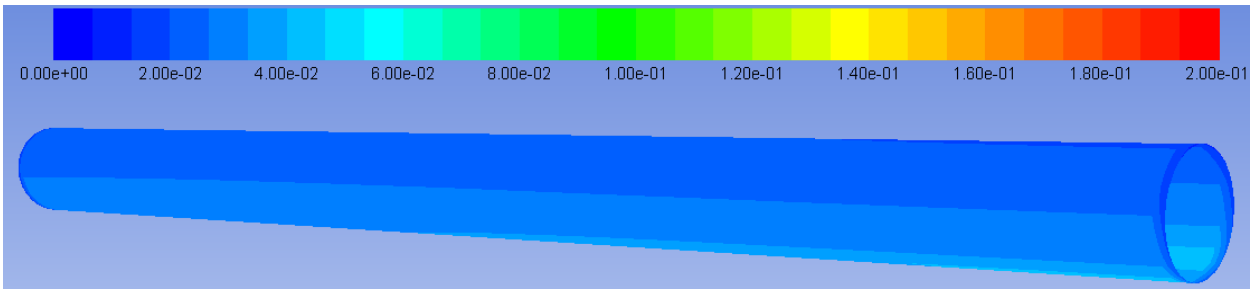

(c) x_{in} = 0.6

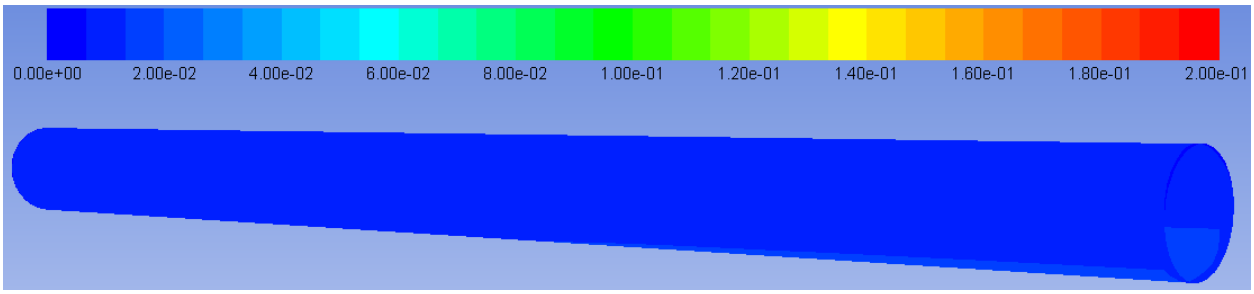

(d) x_{in} = 0.8

Fig. 5

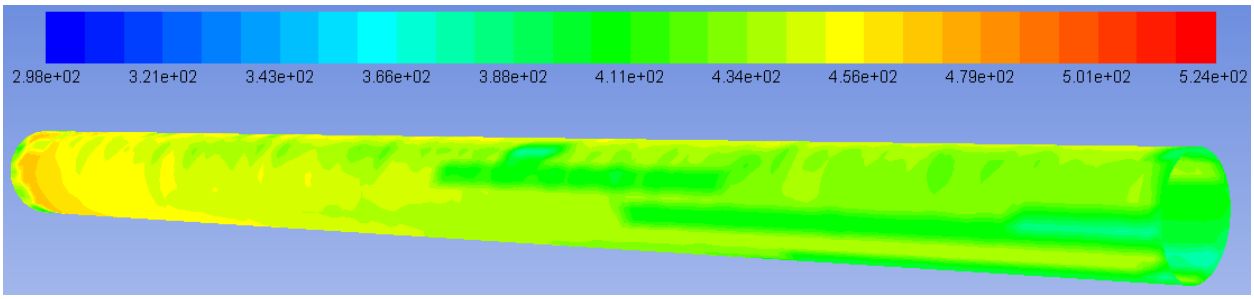

(a) x_{in} = 0.2

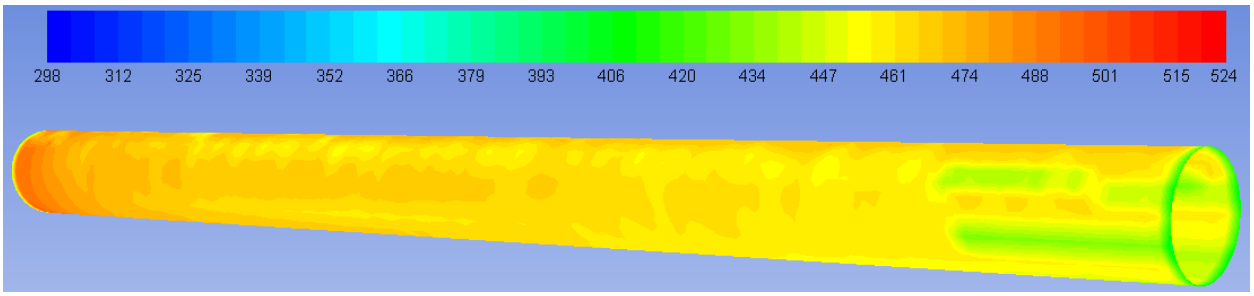

(b) x_{in} = 0.4

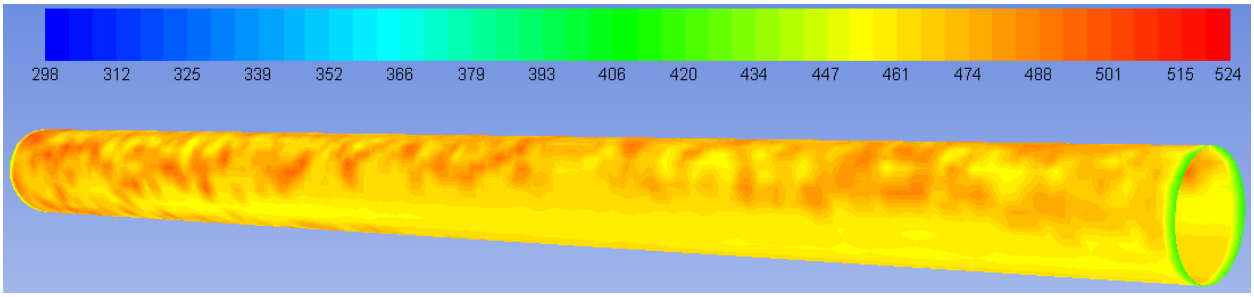

(c) x_{in} = 0.6

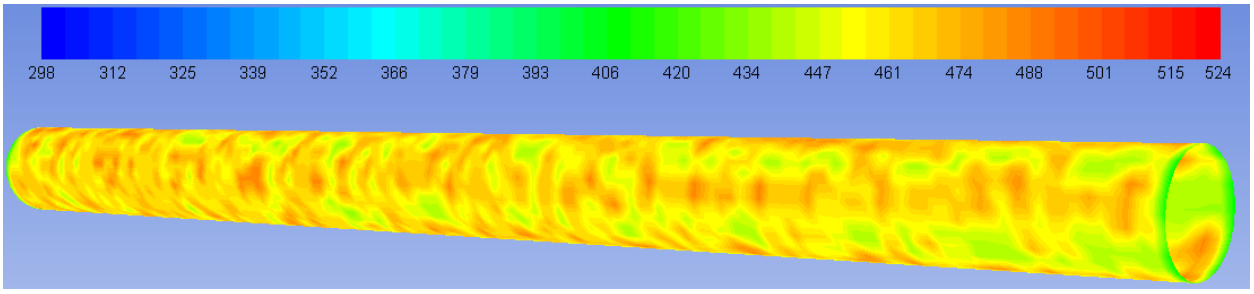

(d) x_{in} = 0.8

Fig. 6

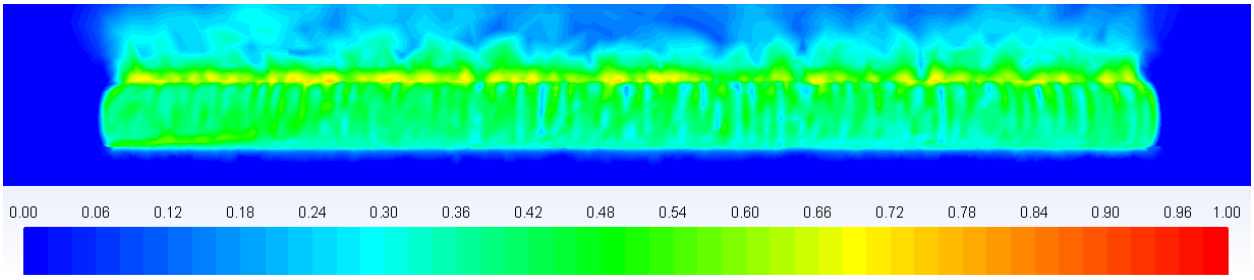

(a) x_{in} = 0.2

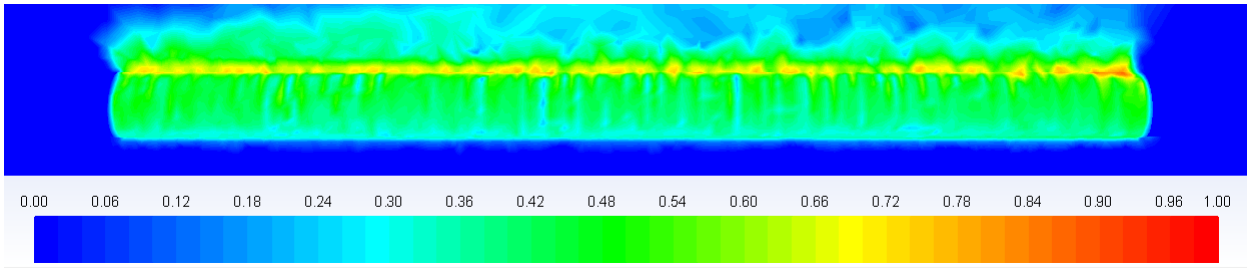

(b) x_{in} = 0.4

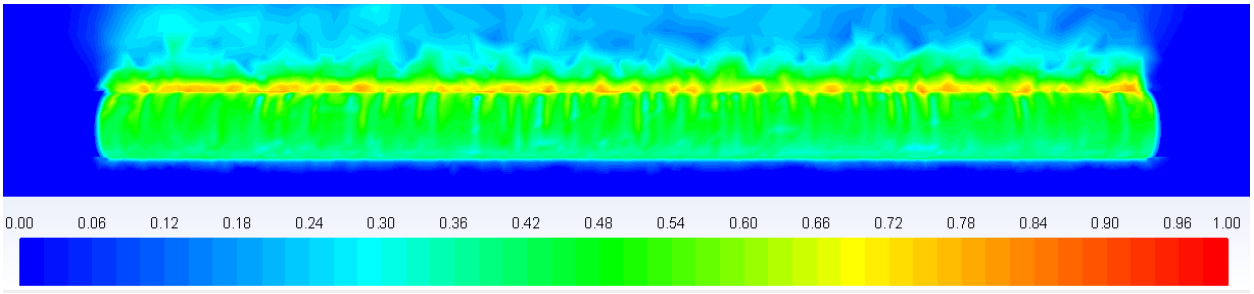

(c) x_{in} = 0.6

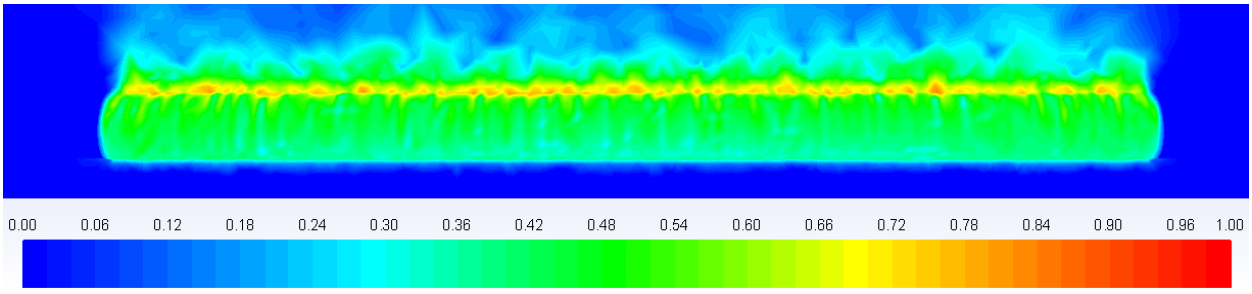

(d) x_{in} = 0.8

Fig. 7

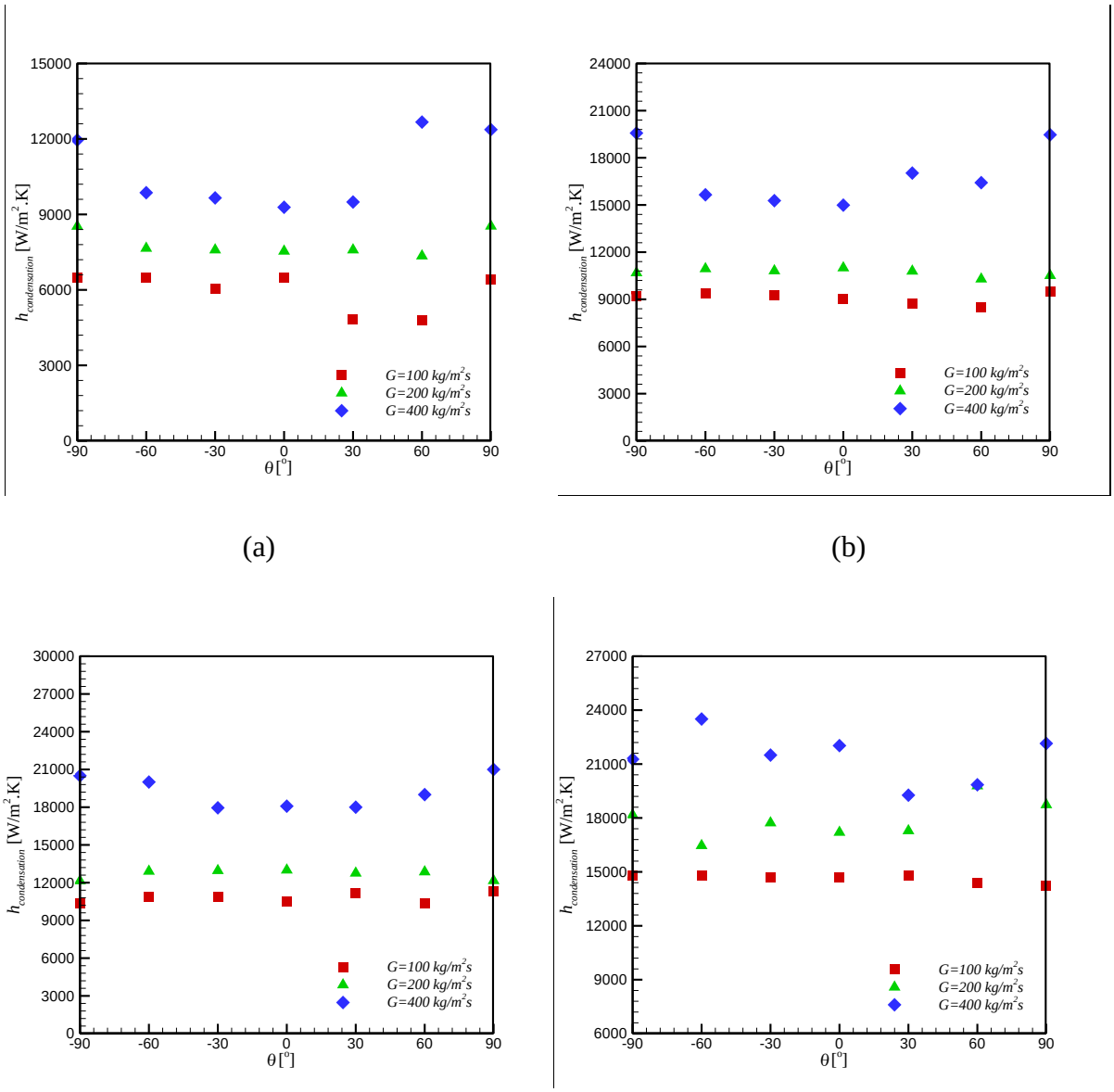
15000
12000
9000
6000
3000
0
$h_{condensation}$ [W/m^2.K]
-90
-60
-30
0
30
60
90
θ[°]
G=100 kg/m^{2}s
G=200 kg/m^{2}s
G=400 kg/m^{2}s
(a)
24000
21000
18000
15000
12000
9000
6000
3000
0
$h_{condensation}$ [W/m^2.K]
-90
-60
-30
0
30
60
90
θ[°]
G=100 kg/m^{2}s
G=200 kg/m^{2}s
G=400 kg/m^{2}s
(b)
30000
27000
24000
21000
18000
15000
12000
9000
6000
3000
0
$h_{condensation}$ [W/m^2.K]
-90
-60
-30
0
30
60
90
θ[°]
G=100 kg/m^{2}s
G=200 kg/m^{2}s
G=400 kg/m^{2}s
(c)
27000
24000
21000
18000
15000
12000
9000
6000
$h_{condensation}$ [W/m^2.K]
-90
-60
-30
0
30
60
90
θ[°]
G=100 kg/m^{2}s
G=200 kg/m^{2}s
G=400 kg/m^{2}s
(d)

Fig. 8

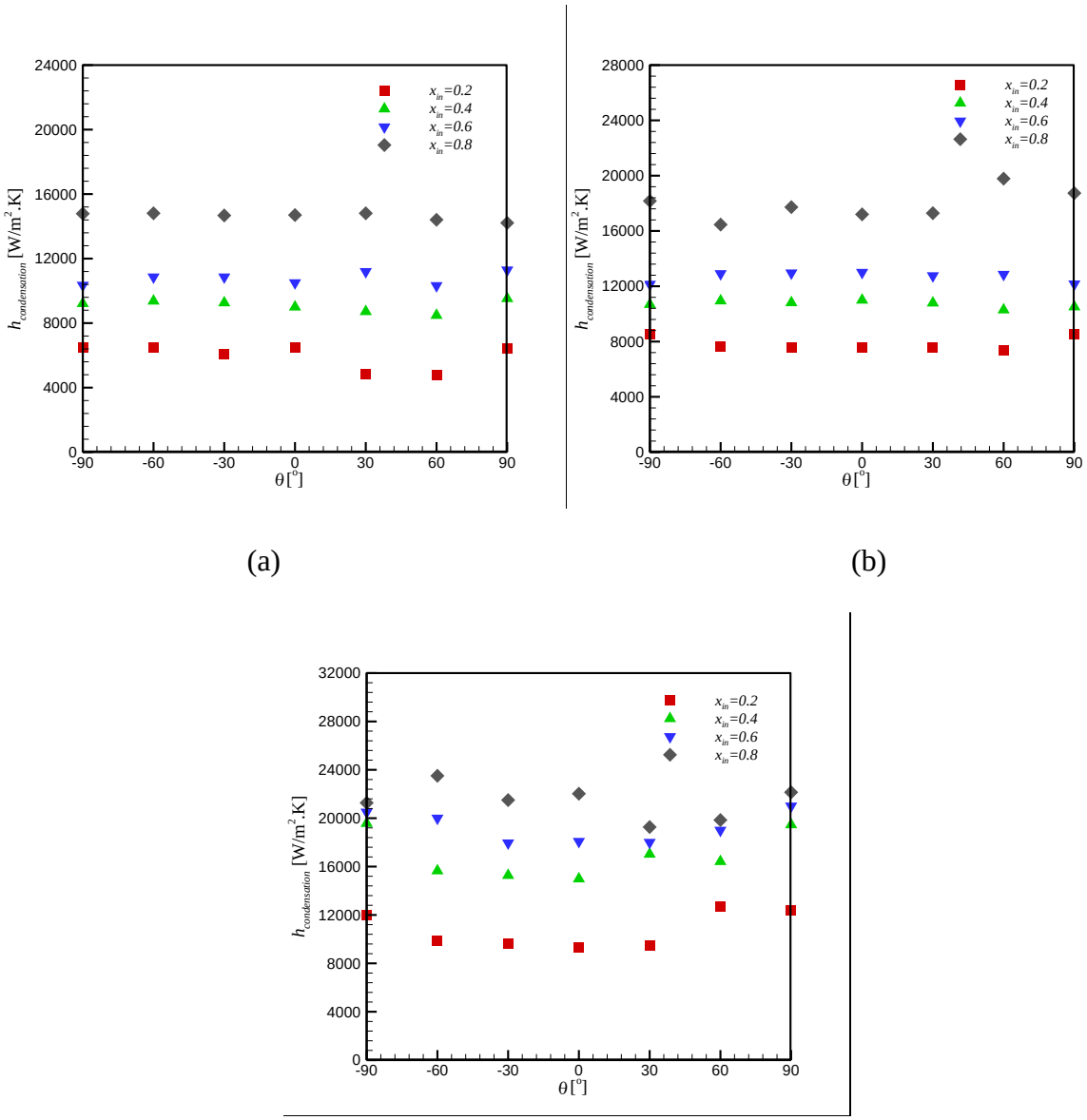

Fig. 9

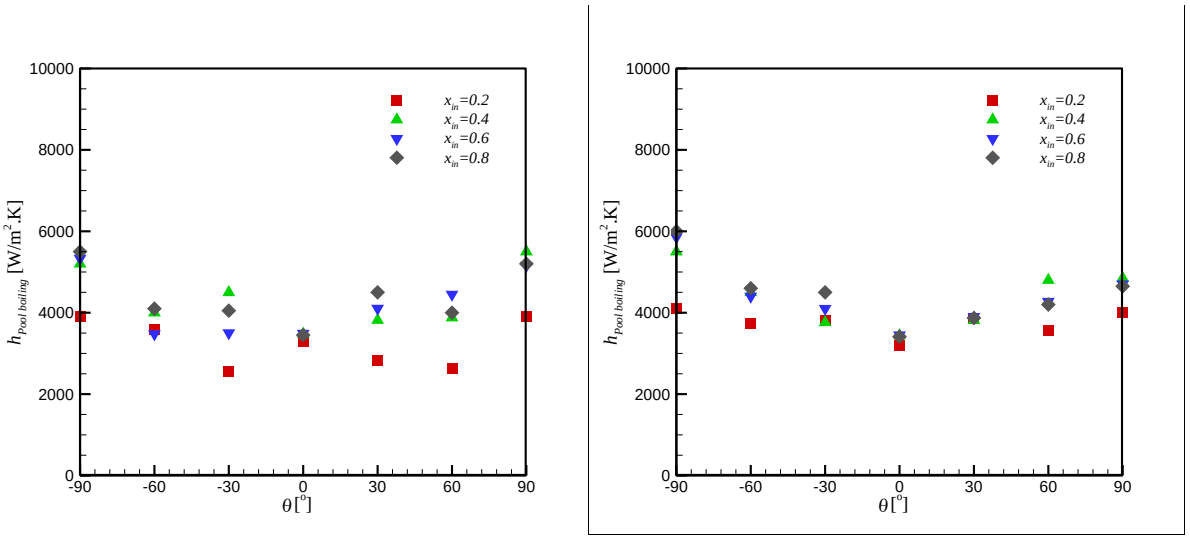
10000
8000
6000
4000
2000
0
-90
-60
-30
0
30
60
90
θ[°]
h_Pool boiling [W/m².K]
x_in=0.2
x_in=0.4
x_in=0.6
x_in=0.8

(a) (b)

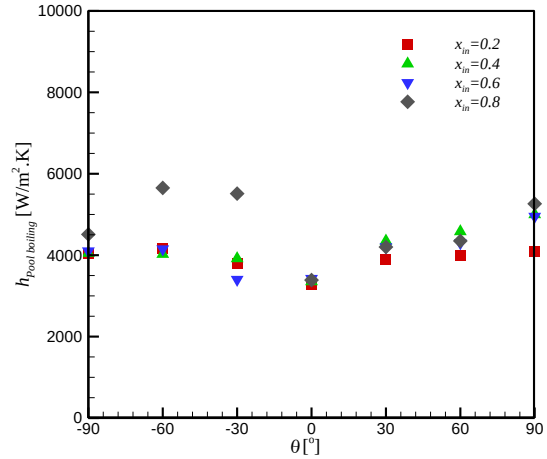
10000
8000
6000
4000
2000
0
-90
-60
-30
0
30
60
90
θ[°]
h_Pool boiling [W/m².K]
x_in=0.2
x_in=0.4
x_in=0.6
x_in=0.8

(c)

Fig. 10

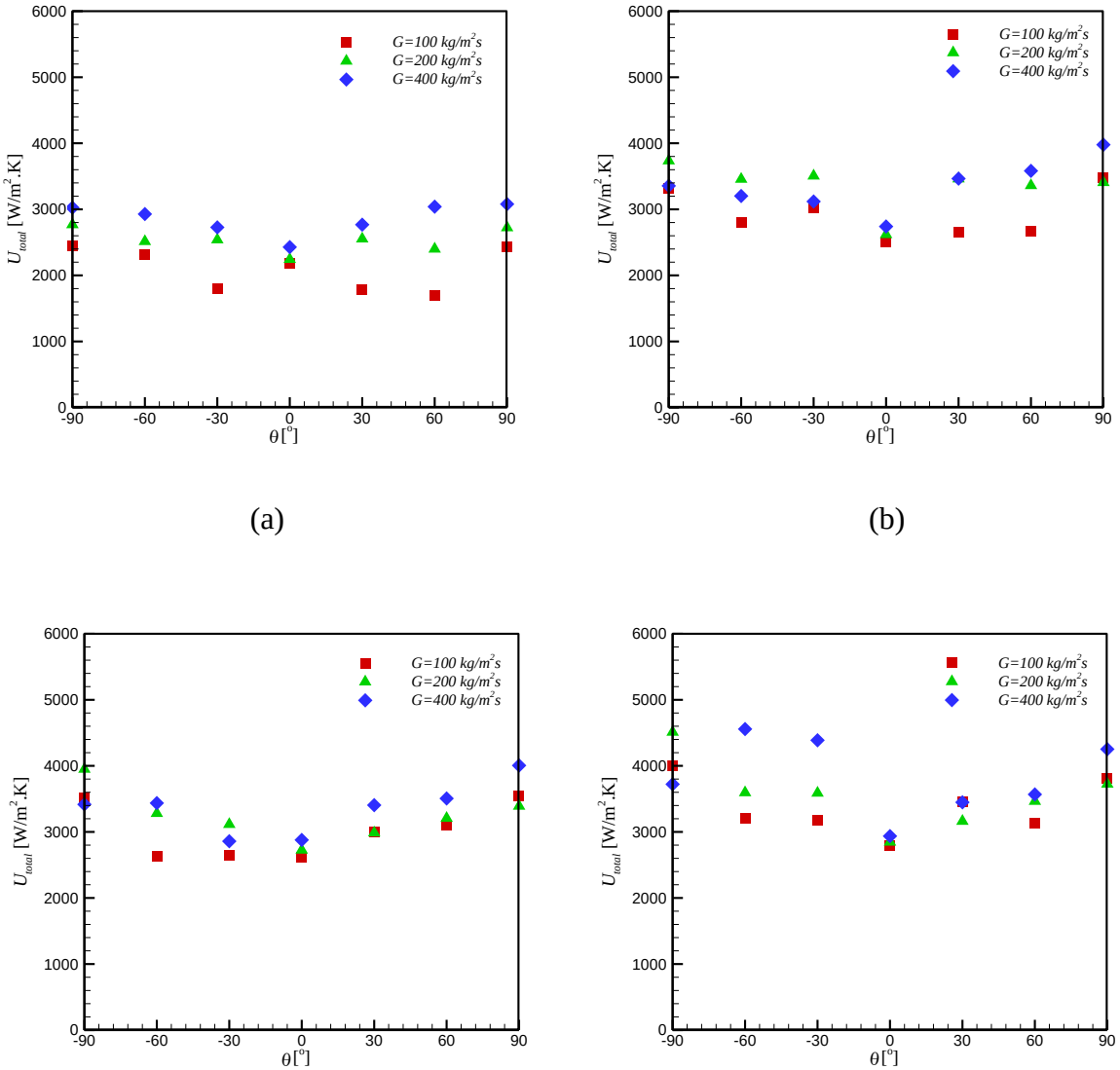

Fig. 11

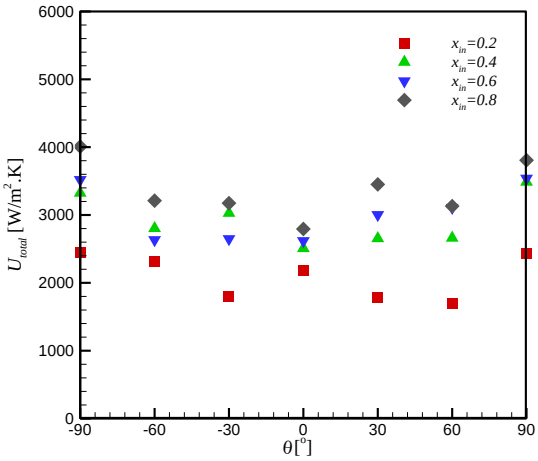
U_{total} [W/m^2.K]
θ[°]
x_{in}=0.2
x_{in}=0.4
x_{in}=0.6
x_{in}=0.8

(a)

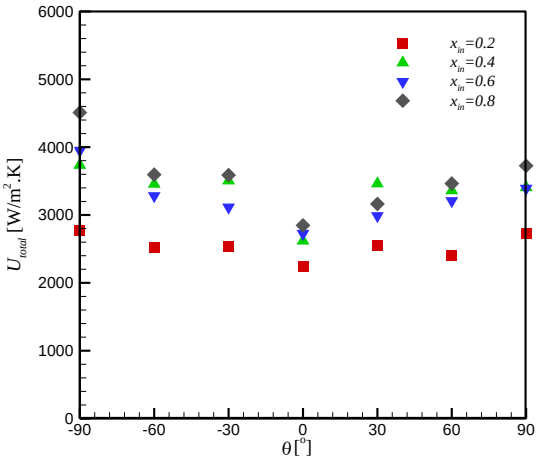
U_{total} [W/m^2.K]
θ[°]
x_{in}=0.2
x_{in}=0.4
x_{in}=0.6
x_{in}=0.8

(b)

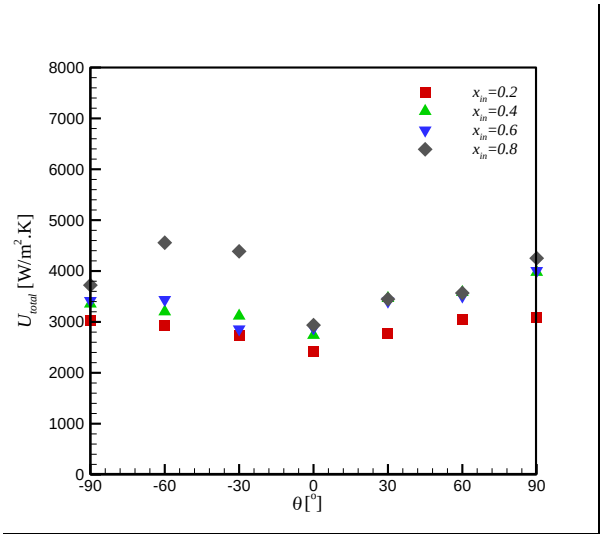
U_{total} [W/m^2.K]
θ[°]
x_{in}=0.2
x_{in}=0.4
x_{in}=0.6
x_{in}=0.8

(c)

Fig. 12

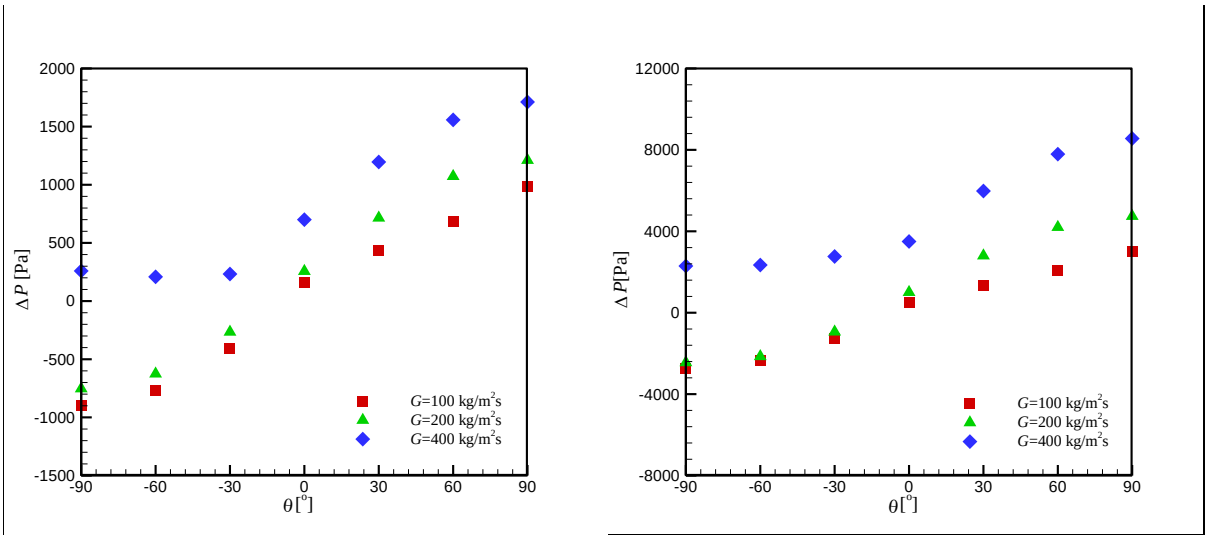
2000
1500
1000
500
0
-500
-1000
-1500
ΔP [Pa]
-90
-60
-30
0
30
60
90
θ[°]
G=100 kg/m²s
G=200 kg/m²s
G=400 kg/m²s
12000
8000
4000
0
-4000
-8000
ΔP[Pa]

(a) (b)

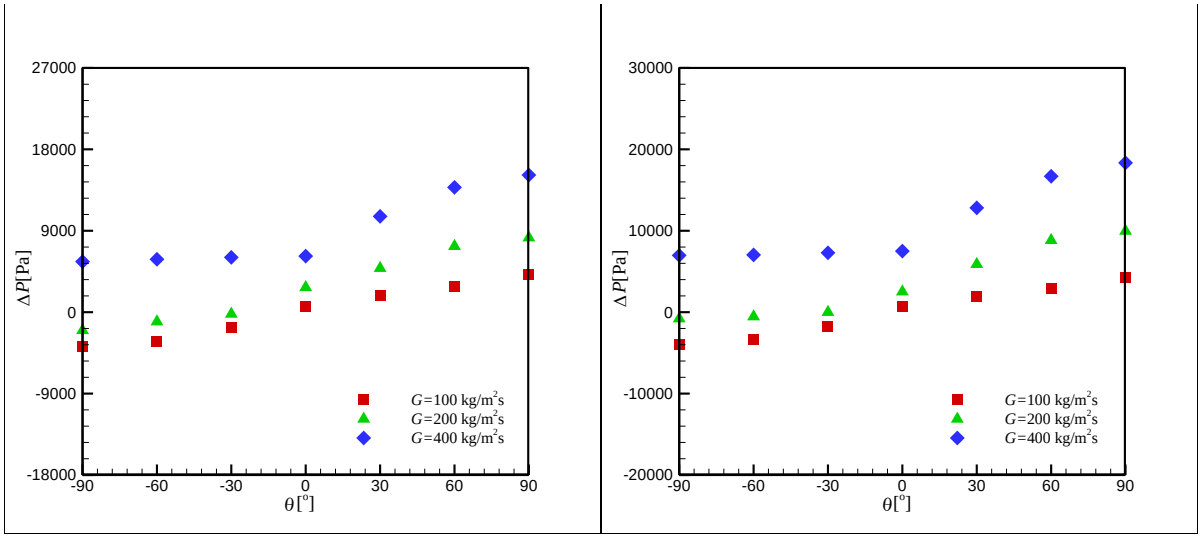
27000
18000
9000
0
-9000
-18000
ΔP[Pa]
-90
-60
-30
0
30
60
90
θ[°]
G=100 kg/m²s
G=200 kg/m²s
G=400 kg/m²s
30000
20000
10000
0
-10000
-20000

(c) (d)

Fig. 13

Tables:

Table 1. Different operating conditions considered in the simulations.

Parameters	**Range**
G_{steam} **[kg/m^{2}s]**	100 - 400
θ **[°]**	-90 - +90
$T_{sat,\ inside\ tube}$ **[°C]**	250
$T_{sat,\ pool}$ **[°C]**	100
x_{in} **[-]**	0.2 - 0.8